Chapter

Twin Boundary in hcp Crystals: Quantum and Thermal Behavior

Victor A. Lykah and Eugen S. Syrkin

Abstract

The 180° twin boundary (TB) (stacking fault) is investigated in the hexagonal close-packed (hcp) light materials. It is shown that atomic symmetry inside the twin boundary is lower than in hcp phase due to interatomic interaction between neighbors. In the case of quantum or thermal behavior, for the isosurfaces, an initial spherical form (in hcp phase) transforms into ellipsoid (in the boundary). We introduce the isosurface deformation parameter. The self-consistent description is developed to estimate the parameters of the thermodynamic potential, and the models of hard spheres and ellipsoids are used. It is shown that the quantum or thermal behavior of the boundary atoms causes the following effects: (i) the increase of degree of overlap of the atomic wave functions or trajectories within the twin boundaries, (ii) the increase of diffusion inside the twin boundaries, and (iii) the decrease of energy and broadening of the quantum boundary in comparison with the classical case.

Keywords: solid helium, twin boundary, stacking fault, hard ellipsoids, quantum diffusion
PACS numbers: 61.72.Mm, 61.72.Nn, 64.75.Gh, 66.30.Ma

1. Introduction

Helium crystals have unique quantum properties and are useful for the investigation of dynamic and kinetic behavior of atomic crystals [1]. In experiments, the structure phase transition between body-centered cubic (bcc) and hcp phase was found for both metals and solid ^{4}He [2, 3]. The coherent phase boundary (PB) and twin boundary (TB) or stacking fault (SF) was investigated theoretically in the frame of one order parameter (OP) model [4, 5]. The two-OP theory of PB [6, 7] was developed on the basis of the Burgers mechanism. In work [5] we proposed the three-OP theory that combines Sanati [6, 7] and Kaschenko [8] treatments; so we take into account the changes of volume and pressure under the phase transition. The three-OP and one-OP descriptions of PB and TB are uniquely related. In different models of coherent bcc-hcp boundary, the local oscillations spectra of OP in ^{4}He were investigated in [9].

In the experiment [10], a glass formation under deformation of solid helium was investigated. Usually the deformation of crystals generates the different defects [11], including stacking faults. In the nuclear magnetic resonance (NMR) experiments [12], the great role of the interface in increasing the quantum diffusion was found. In work [13] for single hcp crystal ^{4}He, the stacking fault energy was measured.

The present work is devoted to the development of the self-consistent description of quantum behavior of ^{4}He atoms in twin boundary proposed in work [14]. We apply this treatment to quantum and thermal description of twin boundary in some metals.

2. Model of the twin boundary

In the hcp phase of crystal ^{4}He, we consider the twin boundary under transition from the close packing layers ABAB ... (see **Figure 1a,b**) to the close packaging ACAC .... The twin boundary (TB) corresponds to stacking faults (SF). The atomic plane A creates different positions (potential wells) B and C for neighbor layers (see **Figure 1a,b**).

The twin boundary was researched in works [4, 5] where the triple-well thermodynamic potential was used. Far from the bcc-hcp transition, the double-well free energy can be applied:

$$F(\xi) = \int \left[\frac{\alpha}{2} \left(\frac{d\xi}{dz} \right)^2 + \frac{k_4 \xi^4}{4} - \frac{k_2 \xi^2}{2} \right] dv, \tag{1}$$

where the integration is over the volume v, square brackets contain the volume energy density, z is a coordinate in the direction of heterogeneity, α is a dispersion parameter responsible for the boundary width, and phenomenological parameters k_4, k_2 are positive. In hexagonal lattice, ξ is the order parameter which means the relative displacement of the atomic layers between positions B and C (see **Figure 1a,b**). For the homogeneous part of the free energy Eq. (1), the maximum and minima positions are

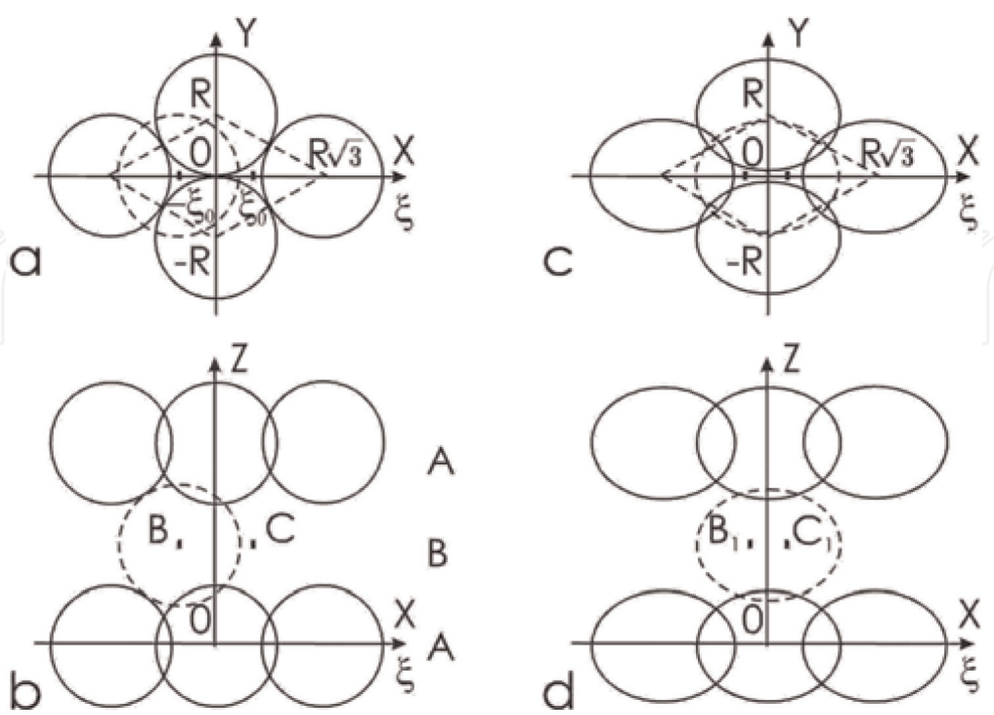

Figure 1.
(a, b) The close pack of the atomic layers (0001) ABAB... for hcp phase. Layer A is shown by solid lines, and layer B is shown by dotted lines. (a) The view perpendicular to the layers. (b) The view along the layers. Points B and C are atomic equilibrium positions in corresponding layer. (c, d) The change in the close packing of the atomic ellipsoids inside TB under quantum effects is accounted.

$$\xi_{max} = 0; \qquad F(\xi_{max}) = 0;$$
$$\xi_{min} = \pm\xi_0; \quad F(\xi_{min}) = -V\frac{k_4\xi_0^4}{4}; \qquad \xi_0 = \sqrt{\frac{k_2}{k_4}}. \tag{2}$$

where $|\xi_0|$ is the minimum position as displacement between the maximum and minimum positions (B and C in **Figure 1a, b**). The difference between the maximum and minimum energies gives the height h of the potential barrier per unit volume:

$$h = \frac{1}{V}[F(\xi_{max}) - F(\xi_{min})] = \frac{k_4\xi_0^4}{4} = \frac{k_2\xi_0^2}{4}. \tag{3}$$

For further analysis it is convenient to write the free energy Eq. (1) in terms of ξ_0 and h:

$$F(\xi) = \int \left[\frac{\alpha}{2}\left(\frac{d\xi}{dz}\right)^2 + \frac{h}{\xi_0^4}\left(\xi^2 - \xi_0^2\right)^2 - h\right]dv. \tag{4}$$

The free energy Eq. (4) gives rise to such one-dimensional inhomogeneity as twin boundary [9, 15] which has shape

$$\xi = \pm\xi_0 \tanh\frac{z}{l_T}; \tag{5}$$

$$l_T = \sqrt{\frac{2\alpha}{k_2}} = \frac{1}{\xi_0}\sqrt{\frac{2\alpha}{k_4}}. \tag{6}$$

where the boundary center is chosen at $z = 0$ and l_T is the characteristic width of the boundary. The shear dependence on coordinate Eq. (5) can be substituted into relation Eq. (4). The surface energy density of the twin boundary is obtained by further integration:

$$W_T = \frac{\sqrt{2\alpha k_2^3}}{3k_4} = \frac{4}{3}l_T h. \tag{7}$$

It is expressed through parameters (α, k_2, k_4) of the microscopic double-well potential or macroscopic parameters (l_T, h). The parameters of the thermodynamic potential Eq. (1) can be transformed into the microscopic ones:

$$k_{21} = \frac{4h_1}{\xi_0^2}; \quad k_{41} = \frac{4h_1}{\xi_0^4};$$
$$h_1 = hv_1;\ k_{21} = k_2v_1;\ k_{41} = k_4v_1. \tag{8}$$

Here h_1, k_{21}, and k_{41} are the barrier height Eq. (3), parameters k_2 and k_4 Eq. (1) normalized per unit cell. These equalities are obtained by multiplying h and k_2 or k_4 to the unit cell volume v_1. The characteristic width Eq. (6) $l_T \simeq 1.5nm$ was obtained by molecular dynamic method in [16].

3. Atomic potential in continual description

In hcp lattice, one can find the symmetry axes (along $0z$) of third and sixth orders. In the close-packed layers (x, y), hcp demonstrates isotropic properties of

macroscopic tensors [11, 17]. The isotropic macroscopic tensors exist at appropriate relations $c/a = \sqrt{8}/3$ of unit cell sizes [1, 11]. Inside the perfect hcp phase, an atom is in high symmetric (isotropic) potential:

$$U_{is}(\mathbf{r}) = \frac{1}{2}k_{is}\left(x^2 + y^2 + z^2\right). \tag{9}$$

where k_{is} is isotropic rigidity. The harmonic approximation Eq. (9) is satisfied better for heavier inert atoms or light metals; however, the helium crystal has pronouncedly anharmonic atomic potential [18]. Nevertheless in helium crystals, the harmonic approximation is successfully applied [19, 20].

The isotropic rigidity k_{is} can be divided into two contributions: $k_{is} = k_p + k_{pn}$, where k_p is rigidity in the plane and k_{pn} is rigidity from the interaction with the neighbor planes.

Inside the twin boundary, the neighbor layers are shifted from the symmetric positions, and it causes an anisotropic atomic potential. The previous spherical potential is broken. Then inside the twin boundary, the initial isotropic atomic potential transforms into

$$\begin{aligned} U_{an1}(\mathbf{r}) &= U_{is}(y,z) + U_{an1}(x); \\ U_{is}(y,z) &= \frac{1}{2}k_{is}\left(y^2 + z^2\right);\ U_{an1}(x) = U_p(x) + U_{pn}(x,\xi); \\ U_p(x) &= \frac{1}{2}k_p x^2;\ U_{pn}(x,\xi) = \frac{k_{41}(\xi - x)^4}{4} - \frac{k_{21}(\xi - x)^2}{2}. \end{aligned} \tag{10}$$

where the isotropic potential Eq. (9) splits into two terms. The first term $U_{an1}(x)$ is an anisotropic and nonlinear part of the potential in the shift direction Ox. The second term $U_{is}(y,z)$ is the rest of the isotropic part which is perpendicular to the shift direction. Further, the potential $U_{an1}(x)$ is divided too into $U_p(x)$, the isotropic part, and $U_{pn}(x,\xi)$, the anisotropic one from the neighbor atomic planes. The last turn depends on the layer shift ξ and the small deviation x. Therefore, only term $U_{pn}(x,\xi)$ changes inside TB which is shown in **Figure 2**. The analysis (see [14]) of the term $U_{pn}(x,\xi)$ allows to write the anisotropic atomic potential Eq. (10) in the following simple form:

$$\begin{aligned} U_{an1}(\mathbf{r},\xi) &\simeq U_0(\xi) + c(\xi)x + \frac{1}{2}k_b(\xi)x^2 + \frac{1}{2}k_{is}\left(y^2 + z^2\right); \\ k_b(\xi) &= k_p + k_{pn}(\xi) = k_{is} + 3k_{21}\left(\frac{\xi^2}{\xi_0^2} - 1\right);\ k_{pn}(\xi) = +k_{21}\left(3\frac{\xi^2}{\xi_0^2} - 1\right). \end{aligned} \tag{11}$$

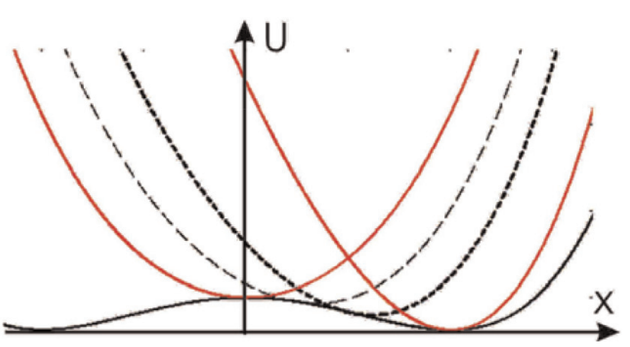

Figure 2.
Smooth changed parts of the potential in dependence on the coordinates ξ and x according to Eqs. (10) and (11): $U_{pn}(0,\xi)$ is a lower double-well curve and $U_{an1}(x,\xi)$ is a set of parabolas.

where $k_b(\xi)$ is rigidity coefficient inside TB, $U_0(\xi)$ is a varied bottom level, and $c(\xi)x$ is the linear part. In the limit points $\xi = \pm\xi_0$, Eq. (11) transforms into isotropic hcp phase Eq. (9) with $k_{pn}(\xi_0) = +2k_{21}$. Inside TB $\xi = 0$, the rigidity takes value $k_{pn}(0) = -k_{21}$. Thus, the rigidity coefficients in phase (k_{is}) and in the middle of TB $(k_b(0))$ are represented by the rigidity coefficients inside the plane (k_p) with two adjacent (k_{21}) planes:

$$k_{is} = k_p + k_{pn}(\xi_0) = k_p + 2k_{21}; \tag{12}$$

$$k_b(0) = k_p + k_{pn}(0) = k_p - k_{21}. \tag{13}$$

Inside the boundary the potential is considerably softer in direction Ox because of $k_b(\xi) < k_{is}$ (see **Figure 2**). The difference in these rigidity coefficients is too high $k_{is} - k_b(0) = 3k_{21}$. For further analysis, we need especially the quadric form in Eq. (11).

The ratio of the rigidity coefficients in the relation Eq. (10) can be related to the ratio of the elastic modules which are shown in **Table 1**. The macroscopic tensor components $C_{11}C_{33}$ describe the longitudinal deformation along the axes $0x$ and $0z$, respectively. In solid ^{4}He, the ratio of the elastic modulus $C_{33}/C_{11} = 1.37$ gives anisotropy of the rigidity coefficients k_{elz}/k_{is} in the basal plane and axis $0z$. Uniaxial compression-tension in the basal plane of $0xy$ corresponds to the elastic modulus of C_{11} and atomic rigidity coefficient k_{is}. The shuffle of the basal planes in an arbitrary direction corresponds to elastic modulus C_{44} and atomic rigidity coefficients $2k_{21}$. Therefore, we have the following inequality:

$$\frac{2k_{21}}{k_{is}} = \frac{2k_{21}}{k_p + 2k_{21}} \lesssim \frac{C_{44}}{C_{11}}. \tag{14}$$

4. The atomic potential and hard sphere model in hcp phase

The geometry of the hcp lattice is shown in **Figure 1a**. In the hard sphere model for the hcp plane A (see **Figure 1a,b**), the coordinates of atomic centers are

$$(0, \pm R_0, 0); \quad \left(\pm R_0\sqrt{3}, 0, 0\right); \tag{15}$$

where R_0 is the atomic radius, x is a coordinate along the shift direction of the atomic plane B, z is a coordinate along the direction perpendicular to the atomic plane, and y is a coordinate along the atomic plane perpendicular to the shift direction. (0,0,0) is the touch point of the spheres in plane A. Then the sphere

Element	C_{11}, GPa	C_{33}, GPa	C_{13}, GPa	C_{44}, GPa
^{4}He [21][a]	$4{:}05{\cdot}10^{-2}$	$5{:}54{\cdot}10^{-2}$	$1{:}05{\cdot}10^{-2}$	$1{:}24{\cdot}10^{-2}$
^{7}Li [22][b]	14.2	—	—	10.7
^{9}Be [23][b]	292	349	6	163
^{24}Mg [23][b]	59.3	61.5	21.4	16.4

[a] *The elastic moduli of hcp ^{4}He are found at $T \sim 1$K and molar volume $20.97{\cdot}10^{-6}$m^3/mol [21].*
[b] *At room temperature.*

Table 1.
The experimental values of the elastic moduli of some hcp materials in the notation of Voigt C_{ik} *following [11].*

centers of the shifting atomic plane B can move over the following four spherical surfaces:

$$\begin{aligned} x^2 + (y \pm R_0)^2 + z^2 &= (2R_0)^2; \\ \left(x \pm R_0\sqrt{3}\right)^2 + y^2 + z^2 &= (2R_0)^2; \end{aligned} \tag{16}$$

The equilibrium points for the atom of the shifting neighbor atomic plane B can be found from the geometry of the system (Eq. (16) at y = 0):

$$x_{Re} = \pm R_0 \frac{1}{\sqrt{3}}; \quad y_{Re} = 0; \quad z_{Re} = R_0\sqrt{\frac{8}{3}}. \tag{17}$$

Signs – and + in x_{Re} describe positions B and C in plane B, respectively. From the first Eq. (16), the saddle point coordinates for an atom of plane B are

$$x_{Rs} = 0; \qquad y_{Rs} = 0; \qquad z_{Rs} = R_0\sqrt{3}. \tag{18}$$

For the hard sphere model, the microscopic parameters ξ_0, h_1 are

$$\xi_{0R} = |x_{Re}|; \quad h_{1-R} = \frac{1}{2} g k_{is} (z_{Rs} - z_{Re})^2 \tag{19}$$

where h_{1-R} is the potential barrier between B to C position (see **Figure 1**). Coefficient $g \sim 1$ evaluates the quasielastic energy. In the middle of TB, the neighbor number is 4, which is less than 6 once inside the phase. This is a microscopic reason for the quasielastic energy behavior.

For the hard sphere model, the substitution of relations (19) into Eqs. (3) and (8) gives the parameters of the microscopic interatomic potential:

$$k_{21-R} = \frac{4h_{1-R}}{\xi_{0R}^2}; \quad k_{41-R} = \frac{4h_{1-R}}{\xi_{0R}^4}. \tag{20}$$

For comparison, Eq. (11) allows us to find the rigidity coefficients in the phase k_{is} and in the middle of the boundary $k_b(0)$.

5. Quantum atomic spheres and ellipsoids in hcp phase and in the twin boundary

Inside the perfect hcp phase, a ^{4}He atom is in highly symmetric potential of neighbor atoms. In isotropic harmonic approximation [19, 20], the atomic potential can be presented as [24]

$$U_{is}(\mathbf{r}) = \frac{1}{2} m\omega^2 \mathbf{r}^2; \quad \lambda = \frac{m\omega}{\hbar}. \tag{21}$$

where m, $\mathbf{r}$ and λ are mass, radius vector of ^{4}He atom and parameter of the quantum oscillator. The potential Eq. (12) gives $m\omega^2 = k_{is}$; $\lambda^2 = k_{is}m/\hbar^2$.

The Schrodinger equation splits into three equivalent independent equations with the constant $k^2 = k_X^2 + k_y^2 + k_z^2 = 2mW/\hbar^2$ where k_i are wave numbers. The ground state solution [24] has total zero-point energy $W_{0is} = \frac{3}{2}\hbar\omega$. In isotropic harmonic approximation, a distribution of probability density $\rho = |\psi(x,y,z)|^2$ of

helium atom has spherical symmetry. Hence, the equation of probability isosurface (sphere of radius R) is

$$x^2 + y^2 + z^2 = R^2; \quad R^2 = \frac{N_{\rho is}}{\lambda}; \quad N_{pis} = \ln\sqrt{\frac{\lambda^3}{\rho^2\pi^3}}. \tag{22}$$

The probability density at a distance of R_0 that equals to the radius of the atom in the hcp phase (half the distance between the centers of neighboring atoms in the crystal) is

$$\rho_0 = \sqrt{\frac{\lambda^3}{\pi^3}}\exp\left(-\kappa_0^2\right) \; ; \quad N_{\rho is}(R_0) \equiv \kappa_0^2 = R_0^2\lambda. \tag{23}$$

Here we have introduced the dimensionless parameter κ_0 that is important for further consideration. This parameter is proportional to the atomic radius $\kappa_0 \sim R_0$ and depends on the isotropic rigidity of the atomic lattice $\kappa_0 \sim \lambda^{1/2} \sim k_{is}^{1/4}$. In respect to a huge change in the volume of solid helium [1], the parameter κ_0 can vary widely.

An anisotropic harmonic potential can be written as [24]

$$\begin{aligned} &U_{anis}(\mathbf{r}) = \frac{1}{2}m\left(\omega_X^2x^2 + \omega_y^2y^2 + \omega_z^2z^2\right) \; ; \\ &\lambda_X = \frac{m\omega_X}{\hbar}; \quad \lambda_y = \frac{m\omega_3}{\hbar}; \quad \lambda_z = \frac{m\omega_z}{\hbar}. \end{aligned} \tag{24}$$

The parameters λ_i are related to the rigidity coefficients:

$$\lambda_X^2 = \frac{m}{\hbar^2}k_{xel}; \quad \lambda_y^2 = \frac{m}{\hbar^2}k_{yel}; \quad \lambda_z^2 = \frac{m}{\hbar^2}k_{zel}. \tag{25}$$

In the hcp phase, an anisotropic harmonic approximation is more adequate. Then the rigidity coefficients satisfy inequality $k_{xel} = k_{yel} = k_{is} < k_{zel}$. If we use isotropic harmonic approximation in the hcp phase, then inside of the twin boundary, an atom ^{4}He is in a uniaxial potential of neighboring atoms of Eq. (13): $k_{xel} = k_b \leq k_{yel} = k_{zel} = k_{is}$.

The equation splits also into three independent equations with known solutions [24]. Inside TB for the ground state, the distribution of the probability density of the helium atom loses its spherical symmetry. The probability isosurface is ellipsoid with semiaxes $a \geq b \geq c$:

$$a^2 = \frac{N_\rho}{\lambda_X}; \quad b^2 = \frac{N_\rho}{\lambda_0}; \quad c^2 = \frac{N_\rho}{\lambda_z}; \quad N_p = \ln\sqrt{\frac{\lambda_X\lambda_0\lambda_z}{\rho^2\pi^3}}. \tag{26}$$

Parameter N_ρ describes the probability density. If the probability density equals ρ_0 at the atomic radius R_0 in the hcp phase Eq. (23), then $N(\rho)$ takes the following value:

$$N_{\rho_0} = \kappa_0^2 + \ln\sqrt{\frac{\lambda_X\lambda_0\lambda_z}{\lambda^3}}. \tag{27}$$

Thus, the relations Eqs. (26) and (27) describe the probability density isosurfaces to find an atom in the anisotropic case. On appropriate limit $\lambda_i = \lambda$, these relations describe the isotropic case.

6. Classic atomic thermal spheres and ellipsoids in hcp phase and the twin boundary

Inside the perfect hcp phase, an atom is positioned in highly symmetric potential of neighbor atoms (see Eq. (9)) and quantum analogue Eq. (21). For any direction, the average thermal energy of an atom is $k_BT/2$ where k_B and T are the Boltzmann constant and temperature.

In isotropic harmonic approximation Eq. (9), the average thermal energy of an atom corresponds to the average potential isosurface (sphere of radius R):

$$x^2+y^2+z^2=R^2; \quad R^2=\frac{k_BT}{k_{is}}; \tag{28}$$

The general anisotropic potential has form Eq. (10). In anisotropic harmonic case, the potential can be written with corresponding rigidity coefficients as (compare with Eq. (24))

$$\begin{aligned} &U_{anis}(\mathbf{r})=\frac{1}{2}\left(k_X^2x^2+k_y^2y^2+k_z^2z^2\right);\\ &k_X=k_{xel}; \quad k_y=k_{yel}; \quad k_z=k_{zel}. \end{aligned} \tag{29}$$

Then inside of the twin boundary, an atom is in the uniaxial potential of neighboring atoms Eq. (13): $k_{xel}=k_b\le k_{yel}=k_{zel}=k_{is}$.

The motion equation splits also into three independent equivalent equations. The equation of the potential isosurface is ellipsoid with semiaxes $a\ge b\ge c$ (compare with Eq. (26)):

$$\begin{aligned} &\frac{x^2}{a^2}+\frac{y^2}{b^2}+\frac{z^2}{c^2}=1;\\ &a^2=\frac{k_BT}{k_X}; \quad b^2=\frac{k_BT}{k_y}; \quad c^2=\frac{k_BT}{k_z}. \end{aligned} \tag{30}$$

Thus, the relation Eq. (30) describes the atomic potential isosurfaces in the anisotropic case, i.e., inside TB. In the limit case $k_i=k_{is}$, it corresponds to the isotropic case, i.e., hcp phase Eq. (28). The thermal potential isosurfaces (ellipsoids) have to be in order less than the quantum atomic spheres and ellipsoids normalized at R_0. We emphasize that in this section the average thermal motion of atoms was considered.

7. The self-consistent description of the twin boundary

The **classic description** of TB uses two coefficients of the thermodynamic potential Eq. (1):

$$k_{21}=const; \qquad k_{41}=const; \quad \text{or } h_1=const; \qquad \xi_0=const. \tag{31}$$

They can be corresponded to the hard sphere model (see Eqs. (15)–(20)).

The quantum and thermal description of TB is self-consistent, i.e., the parameters Eq. (31) are varied as a function of some parameter q that, in its turn, is a function of these parameters:

$$h_1=h_1(q); \qquad \xi_0=\xi_0(q); \qquad q=q(h_1,\ \xi_0). \tag{32}$$

Let us introduce the **isosurface deformation parameter** q as a geometric factor which describes the deformation of the atomic sphere Eqs. (22) and (28) into the one-axis ellipsoid Eqs. (26) and (30):

$$q = 1 - \frac{c^2}{a^2} \equiv \varepsilon^2; \quad 0 \le \varepsilon^2 \le 1. \tag{33}$$

where ε is the eccentricity of the ellipse. Earlier in the paper [14], we introduced the quantum deformation parameter q_q. Here we generalize the parameter q_q to the cases of either quantum or thermal motion of an atom and introduce the isosurface deformation parameter q.

Now we present the self-consistent scheme of description for the twin boundary.

(0) Zero approximation. An atom is a hard classic sphere Eq. (32) or quantum isotropic oscillator:

$$R_0 = a = b = c; \quad \rho = \rho_0; \quad q = 0. \tag{34}$$

(1) The first approximation. An atom is considered as a quantum anisotropic uniaxis oscillator. The potential Eq. (10) has been obtained in zero approximation. In the general case, the ellipsoid parameters and the isosurface deformation parameter are described by Eqs. (26), (27), and (33), respectively. The long ellipsoids axis is oriented along the shift direction $0x$:

$$b_1 = c_1 < a_1; \quad \rho = \rho_0; \quad \varepsilon_{c1}^2 = q_1 = 1 - \frac{c_1^2}{a_1^2} > 0. \tag{35}$$

The further variations of **parameters** Eq. (31) can be obtained in the hard ellipsoid model. The hard ellipsoids have the isosurfaces with the same probability density ρ_0 as the hard spheres in the hcp phase, and the isosurface deformation parameter can be obtained. For a vacancy, the nearest neighbors form similar ellipsoids [25].

(2) The second approximation. An atom is considered as an anisotropic three-axis oscillator (the isosurface is three-axis ellipsoid). The first approximation gives the rigidity coefficients of the potential. Different ellipses are formed in the planes ab and ac, and their eccentricities equal

$$b_2 \neq c_2 < a_2; \quad \varepsilon_{b2}^2 = q_{b2} = 1 - \frac{b_2^2}{a_2^2} > 0; \quad \varepsilon_{c2}^2 = q_{c2} = 1 - \frac{c_2^2}{a_2^2} > 0. \tag{36}$$

Now all three axes of the atomic ellipsoid are different. The softest potential and the longest axis a_2 are still oriented along the shift direction. The hard ellipsoid model Eq. (35) is used to obtain a new local atomic potential and a new ellipsoid shape.

(i) The third and further i^{th} steps qualitatively replicate the previous steps in the same way. The second and further steps are more cumbersome and complicated.

8. Atom as anisotropic harmonic oscillator in the boundary, one axis

In continual description inside the boundary, we have found a change of the atomic potential Eq. (10) with the corresponding rigidity constants. Therefore, constants λ_i in Eq. (25) take the following forms:

$$\lambda_X = \frac{1}{\hbar}\sqrt{m\left[k_{is} + 3k_{21}\left(\frac{\xi^2}{\xi_0^2} - 1\right)\right]} \leq \lambda; \quad \lambda_y = \lambda_z = \lambda = \frac{1}{\hbar}\sqrt{mk_{is}}. \tag{37}$$

Using Eqs. (26) and (27), the atomic isosurface can be described by ellipsoid with semiaxes:

$$a_1^2 = \frac{N_{\rho_0 1}}{\lambda_X}; \quad b_1^2 = c_1^2 = \frac{N_{\rho_0 1}}{\lambda}; \quad N_{\rho_0 1} = \kappa_0^2 + \ln\sqrt{\frac{\lambda_X}{\lambda}}. \tag{38}$$

For fixed $\lambda_y, \lambda_z = \lambda$ and reduced stiffness coefficient λ_X along axis $0x$, the semiaxes of the ellipsoid change as follows: $a_1 > R_0$; $b_1 = C_1 < R_0$. Then the isosurface deformation parameter q_1 Eq. (35) takes the following dependence on the order parameter ξ and coordinate

$$q_1 = 1 - \sqrt{1 - 3\frac{k_{21}}{k_{is}}\frac{1}{\cosh^2(z/l_T)}}. \tag{39}$$

We obtain the same result for the thermal excitations; however, instead of relation Eq. (37), we use the rigidity constants Eq. (30):

$$k_X = k_{is} + 3k_{21}\left(\frac{\xi^2}{\xi_0^2} - 1\right) \leq k_{is}. \tag{40}$$

In **Table 2**, evaluations of different parameters are shown according to **Table 1** and relation Eqs. (14), (39), (42), and (43); the sources are shown in round brackets on top of columns.

In He and Mg (see **Table 2**), the transverse components of the elastic module C_{44} are much smaller than the longitudinal ones C_{11}. Accordingly in these materials, the isosurface deformation parameters in the middle point of TB q_{max} take relatively small value.

In Li and Be (see **Table 2**), the transverse and longitudinal components of the elastic moduli are closer. Hence, in these materials, the parameters q_{max} are considerably greater. Moreover in Li, the parameter q_{max} can reach 1 or even take complex (imaginary root) values. This indicates a possible instability of Li crystal lattice (see further consideration). This, seemingly unexpected, result is quite understandable

Element	$\frac{C_{44}}{C_{11}}$, (Table 1, (14))	$3\frac{k_{21}}{k_{is}}$, Eq. (14)	q_{max}, Eq. (39)	κ_0^2, Eq. (42)	Λ, Eq. (43)
^{4}He	$\simeq 0.306$	≤ 0.46	$\simeq 0.27$	$\simeq 3.77$	$\simeq 0.0663$[a]
^{7}Li[b]	$\simeq 0.75$	≤ 1.13	$\rightarrow 1$	$\simeq 151.3$	$\simeq 0.0017$[c]
^{9}Be[b]	$\simeq 0.558$	≤ 0.84	$\simeq 0.60$	$\simeq 127.4$	$\simeq 0.0020$[c]
^{24}Mg[b]	$\simeq 0.277$	≤ 0.41	$\simeq 0.23$	$\simeq 353.4$	$\simeq 0.0007$[c]

[a] *Evaluation of the de Boer parameter $\Lambda = 0.45$ for ^{4}He at ~1 K [2].*

[b] *At room temperature.*

[c] *Evaluation of the de Boer parameter at ~ 1K (present work).*

For all materials the parameters κ_0^2 and Λ are evaluated with the same R_0.

Table 2.
Evaluation of the elastic moduli relations, rigidity relations, the isosurface deformation parameter in the middle point of TB q_{max}, and the de Boer parameter Λ of some hcp materials.

if considerably gentle upper parabolas (stronger interaction between the crystal planes in comparison with in-plane interaction) are taken into account which are shown in **Figure 2**.

In the quantum case, we can evaluate the minimal increase of the exchange integral due to the increase of overlapping wave functions caused by the elliptic deformations [14]:

$$\begin{aligned} \Delta I &= \Delta I_0 = \frac{1}{\cosh^4(z/l_T)}; \\ \Delta I_0 &= \frac{3}{16\sqrt{\pi}} \frac{1}{4\sqrt{\kappa_0^5}} \left(\frac{k_{21}}{k_{is}}\right)^2 \exp\left(-\kappa_0^2\right); \end{aligned} \tag{41}$$

Increasing overlapping volumes ΔV with high probability can be evaluated by segments of the crossing ellipsoids. Amplitude ΔI_0 depends on two parameters κ_0 and k_{21}/k_{is} only.

In the basal hcp plane, the exchange integral is varied depending on the quantum deformation parameter q; the wave function tails are the most sensitive, especially in the overlapping region. Evaluations Eq. (41) take into account only space changing but not the amplitude one. The amplitude changing can achieve several orders because of exponential dependence. The exchange integral I uniquely defines the diffusion coefficient [26]. In the interphase boundaries in solid helium, NMR experiment [12] shows the quantum diffusion increasing. The interphase and twin boundaries are similar [5]. So for the quantum diffusion case in TB, the predicted and the experimentally observed arising values are closely related. Experiments show thermal diffusion arising at boundaries [11]; the found thermal ellipsoids' deformation qualitatively explains these facts.

Now we can point out conditions when exchange integral Eq. (41) increases. We need minimal κ_0^2 Eq. (42) in exponent Eq. (41). The parameter κ_0 or λ can be defined by Eqs. (23) and (37) and analyzed in dependence on different factors. In [14] using atomic mass m_a and evaluation of atomic radius R_0, the parameter κ_0^2 value was estimated:

$$\kappa_0^2 \simeq \frac{1}{\hbar} R_0^{5/2} \sqrt{\frac{1}{2} \pi m_a E}. \tag{42}$$

where elastic module $E = C_{11}$ is related to the rigidity coefficient $k_{is} \simeq \pi R_0 E/2$. In solid ^{4}He, the atomic radius R_0 is the soft parameter, especially under low pressure. So, a high value of exchange integral can be achieved. Compressibility is small in metals, first of all, in light ones (lithium, beryllium, magnesium). Minimal rigidity k_{is} gives rise in the exchange integral too. The van der Waals interaction in ^{4}He is 3–4 orders of magnitude less than in metal (see **Table 1**).

Another way to estimate κ_0^2 is to compare it with de Boer parameter Λ, the fundamental characteristic of quantum crystal. The de Boer parameter gives the probability density to find an atom in the site of a neighboring atom (at distance $a_l = 2R_0$) [26]:

$$\rho(a_l) \sim \exp\left(-\frac{1}{\Lambda}\right) = \exp\left(-\lambda a_l^2\right) \;\; ; \;\; \kappa_0^2 = \frac{1}{4\Lambda}. \tag{43}$$

The de Boer parameter $\Lambda = 0.45$ for ^{4}He [26] gives evaluation $\kappa_0^2 \simeq 0.59$. Pressure growing leads to more difficult tunneling of atoms and different κ_0^2 evaluations in Eqs. (42) and (43). Using the data in **Table 1**, for solid ^{4}He we obtain R_0 [14], $\kappa_0^2 \simeq 3.77$, and $\Lambda \simeq 0.07$ (see **Table 2**).

We can make the following conclusion. The softening of the effective atomic potential is anisotropic inside the twin boundary which increases the exchange integral and tunneling probability in the selected shear direction. As a result the quantum diffusion along the boundary plane increases.

9. The self-consistent correspondence of the potential and the uniaxial hard ellipsoid model

Inside the twin boundary, the arising anisotropic atomic potential transforms an atomic probability isosurface from sphere to ellipsoid. Let us introduce the hard ellipsoid model as analogue of the hard sphere model. Then coefficients' local values for the potential can be found inside TB. We suppose that the twin boundary does not change symmetry and positions of the atomic centers inside a shifting plane. So, the atomic plane A keeps the atomic centers' coordinates Eq. (15) under shifting (see **Figure 1c, d**). In the shifting neighbor atomic plane B, the atomic isosurface equation is defined by Eq. (22). Then for the shifting atomic plane B, the atomic (ellipsoids) center moves over the great ellipsoidal surfaces:

$$\begin{gathered}\left(\frac{x}{2a_1}\right)^2+\left(\frac{y\pm R_0}{2c_1}\right)^2+\left(\frac{z}{2c_1}\right)^2=1;\\ \left(\frac{x\pm R_0\sqrt{3}}{2a_1}\right)^2+\left(\frac{y}{2c_1}\right)^2+\left(\frac{z}{2c_1}\right)^2=1;\end{gathered} \tag{44}$$

where the equilibrium and saddle points for an atom are located. Only four ellipsoids with centers $(0,\pm R_0,0)$ and $\left(\pm R_0\sqrt{3},0,0\right)$ are described. Axis $0x$ is directed along the shift (see **Figure 1c, d**).

Relations Eq. (26), (27), and (35) define the ellipsoid's semiaxes as function of R_0, q:

$$\begin{gathered}a_1^2=\frac{N_p}{\lambda_X};\quad q_1=1-\frac{\lambda_X}{\lambda};\\ b_1^2=c_1^2=R_0^2\gamma_1(q_1)\ ;\ \gamma_1(q_1)=1+\frac{1}{\kappa_0^2}\ln\sqrt{1-q_1}.\end{gathered} \tag{45}$$

Accounting these relations and condition $y=0$ (see **Figure 1**), we obtain solution for the equation system Eq. (44) and the equilibrium point coordinates for the atom of the plane B. So, in the hard ellipsoid model, we find the microscopic parameters Eqs. (2) and (3) of the atomic potential:

$$\begin{gathered}\xi_{0-1}=|x_{1-e}|=\xi_0\frac{2-3q}{2(1-q)};\quad h_{1-1}\sim\frac{1}{2}k_{is}(z_{1-s}-z_{1-e})^2=\\ =\frac{3h_{1-R}}{\left(3-\sqrt{8}\right)^2}\left[\sqrt{4\gamma_1(q)-1}-\sqrt{4\gamma_1(q)-1-\frac{1}{12}\frac{(2-3q)^2}{1-q}}\right]^2\end{gathered} \tag{46}$$

where h_{1-R} is defined in Eq. (19). These results are valid in the range $0\le q\le 2/3$. At $q_1\to 2/3$ we have $\xi_{0-1}, h_{1-1}\to 0$ and semiaxis relation $a_1/c_1=1/\sqrt{3}$. At $q=2/3$ the hard ellipsoid model needs transition in another state (see [14]). Therefore, inside TB, the change of the atomic wave function leads to the following change of

the interaction potential: the equilibrium displacement and the potential barrier height decrease (see **Figure 3**). However, the potential barrier height decreases much faster. The resulting evolution of the potential Eq. (46) is shown in **Figure 4**. Then from Eqs. (3) and (46), the coefficients of the potential are

$$k_{21-1} = \frac{4h_{1-1}}{\xi_{01}^2}; \quad k_{41-1} = \frac{4h_{1-1}}{\xi_{01}^4}. \tag{47}$$

Thus, the coefficients of the potential (1) for the shift in the direction $0x$ reduce $k_{21} > k_{21-1}(q)$ and $k_{41} > k_{41-1}(q)$. It means softening of the potential in the direction of the plane shuffle. The correspondence between the hard ellipsoid model and the atomic microscopic potential Eqs. (4), (8), and (46) is shown in **Figure 3**. Elliptical deformation of the probability isosurface leads to the transformation of the potential energy of the atom in Eq. (10):

$$\begin{aligned} U_{an2}(\mathbf{r}) &= U_{an2}(y,z) + U_{p2}(x) + U_{pn2}(x,\xi) \ ; \\ U_{an2}(y,z) &= \frac{1}{2}k_{xe2}z^2 + \frac{1}{2}k_{ye2}y^2;\ U_{p2}(x) = \frac{1}{2}k_{p2}x^2; \\ U_{pn2}(x,\xi) &= \frac{k_{41-1}(\xi - x)^4}{4} - \frac{k_{21-1}(\xi - x)^2}{2}; \end{aligned} \tag{48}$$

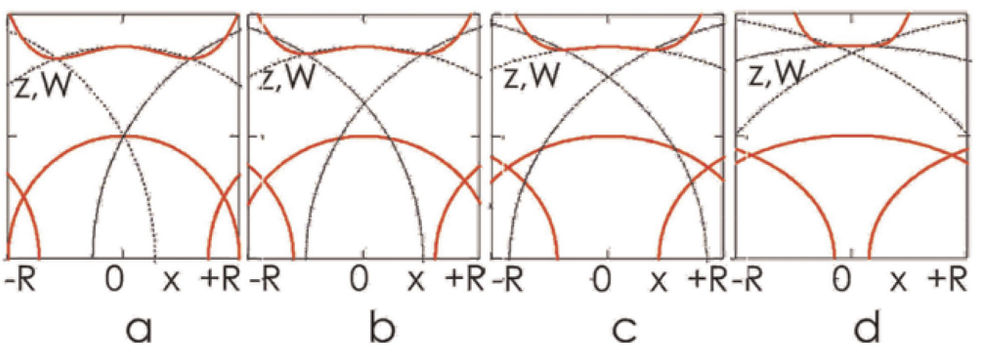

Figure 3.
Comparison of the hard ellipsoids model and the atomic microscopic potential. The red double-well curve shows the potential as a function of ξ_{0-1} and h_{1-1}. Small solid red ellipsoids show atomic isosurfaces at κ_0. Big dot black ellipsoids show the cross sections of the surfaces Eq. (44) at $y = 0$ and quantum parameter values (a) $q = 0$, (b) $q = 0.2$, (c) $q = 0.4$, and (d) $q = 0.6$.

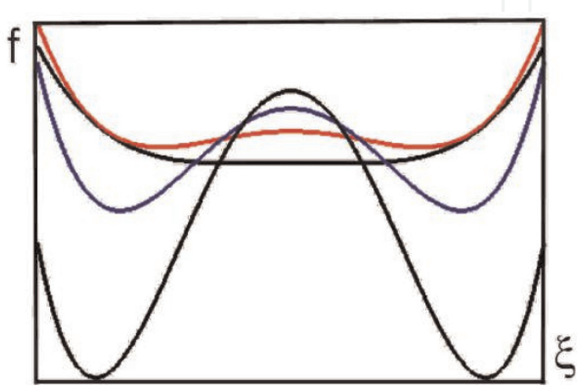

Figure 4.
The cross sections of the potential density according to Eqs. (46), (47), and (39). The quantum boundary has lower potential peak and shorter distance between shallower wells (ξ_{0-1}) as q grows (0, 0.2, 0.4, 0.6). The barrier in the middle of wall (TB) decreases.

All terms are changed in the potential Eq. (48) in comparison with Eq. (10). Isotropy is broken in atomic planes A or B-C due to superposition of the ellipsoids in the shear direction.

For the classical and quantum cases, the free energy density relation Eq. (4) was analyzed analytically in [14]. It was shown that the classical and quantum boundaries have different properties. In particular, from **Figure 5**, it is qualitatively clear why the classical and quantum boundaries have different potential barrier and energy density. In TB both the width and the height of the barrier decrease to zero, according to Eqs. (46) and (47) (see **Figure 4**). In **Figure 3**, they are shown as higher smooth curves. Simultaneously the space width of the boundary $l_T = (1/\xi_0)\sqrt{2\alpha}/k_4$ grows by Eq. (6). The dependence $l_T(q)$ causes further widening of region with $q \to q_{max}$ and a minimal barrier height.

To estimate the energy of the twin boundary (stacking fault) from Eq. (7), we must know the following parameters: α, k_2, k_4 or l_T, h.

The characteristic width (half width) of TB Eq. (6) $l_T \simeq 1.5$ nm was obtained by molecular dynamic method in [16]. We estimate the dispersion parameter α by comparing the differential equations for the transverse sound and shuffling waves:

$$\rho^* \frac{\partial^2 \xi}{\partial t^2} - \alpha \frac{\partial^2 \xi}{\partial z^2} = 0; \quad \frac{\partial^2 u}{\partial t^2} - s^2 \frac{\partial^2 u}{\partial z^2} = 0; \tag{49}$$

where $\rho^* = \rho/2$ is the effective density of the oscillating shuffled subsystem, ρ is the density of helium-4, ξ is the shuffling order parameter, u is macroscopic displacement, and $s = \sqrt{C_{44}}/p \simeq 255$m/s is the transverse sound velocity in the shuffle direction (Oz axis). The velocities of transverse sound and shuffling wave have close values. So the dispersion parameter is $\alpha \simeq C_{44}/2 = 6.2 \cdot 10^6 J/m^3$ where value of module C_{44} is given in **Table 1**.

According to relation Eq. (5), it is possible to estimate the parameter of the thermodynamic potential $k_2 = 2\alpha/l_T^2 \simeq 8.27 \cdot 10^{24}$J/m^5. As follows from Eq. (2) to evaluate the parameter k_4 of the potential, it is necessary to know the maximum displacement of the atom Eq. (17) $\xi_0 = R_0/\sqrt{3} \simeq 1.17 \cdot 10^{-10}$m. Here atomic radius is related to atomic volume: $V_m/N_A \simeq (4/3)\pi R_0^3$. Then $k_4 = 2\alpha/(\xi_0 l_T)^2 = 6.04 \cdot 10^{44}$J/m^7. So, for the classical model of the twin boundary (stacking fault), it is possible to estimate bulk density of the barrier height h and the surface energy density W_T according to Eqs. (3) and (7):

$$h = \frac{k_2 \xi_0^2}{4} \simeq 2.83 \cdot 10^4 J/m^3; \qquad W_T = \frac{4}{3} l_T h \simeq 0.057 mJ/m^2; \tag{50}$$

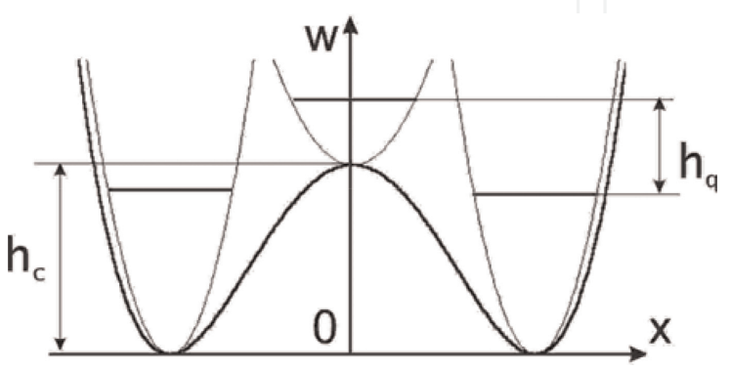

Figure 5.
The smooth double-well potential according to Eqs. (10) and (11). Instead of a set of parabolas in ***Figure 2****, we see only ones at the bottom and the peaks of the potential and their quantum levels. The relationship between the barriers for the atomic displacement in the classical h_c and quantum h_q boundaries is $h_c > h_q$.*

The surface energy density calculated here for the classical model can be compared with the value $W_{SFex} = (0.07 \pm 0.02)\text{mJ/m}^2$ found in the optical experiments at 0.2 K [13].

Above, we have predicted the local reduction of the barrier height h and a local increase in the width l_T of the boundary in the quantum description of the twin boundary (stacking fault). In general for the defect, the surface energy density value $W_T \sim l_{Tef} h_{Tef}$ in Eq. (50) can be close to the classical case. In different experiments and theoretical estimates, a wide variation of the values may be caused by variations of temperatures and pressures.

We have discussed the change of zero vibrations of atoms in the twin boundary (stacking fault) and the related effects. For ^{3}He we can expect the same order of magnitude for all parameters of the twin boundary (stacking fault). The qualitative difference between the pure hcp crystals of isotopes ^{4}He and ^{3}He, apparently, cannot be obtained in the proposed model.

The difference between quantum statistics of the isotopes should address deeper and more delicate quantum properties of the defects. We note briefly below only the most striking manifestation of different statistics and problems arising in this regard.

10. Discussion and conclusion

The quantum self-consistent treatment to twin boundary (stacking faults), proposed in [14] for solid ^{4}He, is developed here for metals and their quantum and thermal description. The relation between discrete models of hard spheres and continuum interatomic potential is used as a sample for a similar relationship in the case of the hard ellipsoid models. As we move deeper into the defect, the transition from one model to another is accomplished.

In the hcp phase, the potential of an atom, created by its neighbors, has spherical symmetry (initial approximation). In the hcp phase, an atom is an isotropic quantum oscillator. In the twin boundary, an atom is an anisotropic quantum oscillator. It is shown that in the twin boundary, the potential of the atom is softer in the direction of shuffle of the atomic planes.

The quantum parameter q_q and its generalization and the isosurface deformation parameter q are introduced. These parameters have simple and visual meaning: q equals to the square of the eccentricity of the cross section of the probability density ellipsoid (or the thermal ellipsoid). We have shown that parameter q is associated with de Boer parameter, the fundamental characteristic of quantum crystal, and anisotropy in the boundary. Evaluations for different materials show that the isosurface deformation parameter q can achieve values 0.2÷1 (see **Table 2**). Meanwhile at $q = 2/3$ the structure instability takes place in the system of the atomic ellipsoids. From this point of view, the properties of TB in lithium are especially interesting because the parameter achieves high value $q \to 1$.

The overlap of the atomic wave functions and the exchange integral value can be described in terms of the quantum parameter q. Inside the twin boundary, the quantum diffusion increases which was observed in the phase boundary (see experiment [12]). The estimation Eq. (50) of the defect energy is in good agreement with experiment [13]. We have shown that the quantum deformation of atoms leads to the space broadening of the twin boundary and to its energy decreasing.

In conclusion we note that local oscillations spectra of the order parameter in different models of coherent bcc-hcp boundary in ^{4}He were investigated in [9]. For small values of the perturbations, dynamical differential equations (reduced to

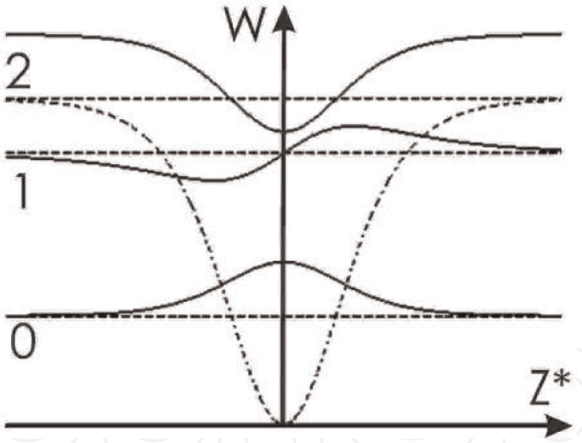

Figure 6.
Local modes of the order parameter at TB [9]. Dash dot line shows the local potential which has local energy levels 0, 1, and 2 (dash). Solid lines show corresponding local oscillations' shape dependence on normalized coordinate z^*.

Schrodinger equations) were obtained and solved. The characteristic frequencies (energy levels) and shape were found and estimated (see **Figure 6**). For the ground state in TB, the local vibration shape can be written as

$$\eta_0(z^*) = \frac{A_0}{\cosh^2 z^*}; \qquad z^* = \frac{z}{l_T}. \tag{51}$$

where A_0 is an amplitude. For the local vibration ground state (51) and for the isosurface deformation parameter q Eq. (39), both shapes coincide qualitatively. In the limit $q << 1$, both coincide completely. The local vibration of the order parameter describes a correlated motion of the atomic layers in twin boundary. Meanwhile, the quantum and thermal treatments give probabilistic descriptions of the atomic motion. The results (the found smooth arising of the atomic motion amplitude in TB) give evidence that different probabilistic (quantum and thermal) and dynamic methods lead to qualitatively identical features of the atomic basic state inside TB.

Acknowledgements

This research is supported by the FFI National Academy of Sciences of Ukraine, grant 4/18-H, Ministry of Science and Education of Ukraine under the Projects M05486 (0118U002048).

Author details

Victor A. Lykah[1*] and Eugen S. Syrkin[2]

1 Educational-scientific Institute of Physical Engineering National Technical University "Kharkiv Polytechnic Institute", Kharkiv, Ukraine

2 B.I. Verkin Institute for Low Temperature Physics of National Academy of Sciences of Ukraine, Kharkiv, Ukraine

*Address all correspondence to: lykahva@yahoo.com

References

[1] Maradudin AA. In: Freiman YA, Manzhelii VG, editors. Physics of Cryocrystals. AIP Press: New York, Woodbury; 1996. p. 691. DOI: 10.1007/1-56396-537-2

[2] Maekawa M, Okumura Y, Okuda Y. Nucleation of crystals at the bcc-hcp transition line in solid ^{4}He. Physical Review B. 2002;**65**:144525. DOI: 10.1103/PhysRevB.65.144525

[3] Birchenko AP, Vekhov EO, Mikhin NP, Polev AV, Rudavskii EY. Kinetics of the bc-chcp transition in ^{4}He off the melting curve. Low Temperature Physics. 2006;**32**:1118-1112. DOI: 10.1063/1.2400684

[4] Lykah VA, Syrkin ES. Twin boundaries as nuclei of a new phase in body-centered cubic-hexagonal close-packed phase transitions in solid helium. Physics of the Solid State. 2010;**52**: 384-391. DOI: 10. 1134/S10637 83410020265

[5] Lykah VA, Syrkin ES. Theory of the phase and twin boundaries in solid helium and reversibility of the bcc-hcp phase transition. Journal of Low Temperature Physics. 2010;**160**: 179-194. DOI: 10.1007/sl0909-0l0-0l9l-6

[6] Sanati M, Saxena A, Lookman T, Alberts RC. Landau free energy for a bcc-hcp reconstructive phase transformation. Physical Review B. 2001;**63**:224114. DOI: 10.1103/PhysRevB.63.224114

[7] Sanati M, Saxena A, Lookman T. Domain wall modeling of bcc to hcp reconstructive phase transformation in early transition metals. Physical Review B. 2001;**64**:092101. DOI: 10.1103/PhysRevB.64.092101

[8] Kaschenko MP, Chaschina VG. Crystal dynamics of the BCC-HCP martensitic transformation: I. controlling wave process. The Physics of Metals and Metallography. 2008;**105**: 537-543. DOI: 10. 1134/S003 1918X08060021

[9] Lykah VA, Syrkin ES. Local oscillations in different models of coherent bcc-hcp boundary in ^{4}He and metals. Physica Status Solidi B. 2011; **248**:1392-1398. DOI: 10. 1002/pssb.201046304

[10] Lisunov AA, Maidanov VA, Rubanskyi VY, Rubets SP, Rudavskii EY, Rybalko AS, et al. Features of the temperature dependence of pressure of solid helium at low temperatures. Low Temperature Physics. 2012;**38**:459-465. DOI: 10.1063/1.4723660

[11] Kittel C. Introduction to Solid State Physics. 8th ed. New York: Wiley; 2004. p. 704

[12] Vekhov EO, Birchenko AP, Mikhin NP, Rudavskii EY. Fast diffusion process in quenched hcp dilute solid ^{3}He-^{4}He mixture. Journal of Low Temperature Physics. 2010;**158**:496-501. DOI: 10.1007/sl0909-009-0022-9

[13] Junes HJ, Alles H, Manninen MS, Parshin AY, Todoshchenko IA. Stacking fault energy in ^{4}He crystals. Journal of Low Temperature Physics. 2008;**153**: 244-249. DOI: 10.1007/sl0909-008-9828-0

[14] Lykah VA, Syrkin ES. Quantum behavior of the twin boundary and the stacking fault in hcp helium crystals. Journal of Low Temperature Physics. 2015;**181**:10-29. DOI: 10.1007/sl0909-015-1328-4

[15] Lines ME, Glass AM. Principles and Application of Ferroelectrics and Related Materials. 2nd ed. Oxford: Clarendon; 2001. p. 683. DOI: 10.1093/acprof:oso/9780198507789.001.0001

[16] Ceperley D. Supersolid: Crystal or plastic? Nature Physics. 2006;**2**:659-660. DOI: 10. 1038/nphys424

[17] Landau LD, Lifshitz EM. Theory of Elasticity. 3rd ed. Vol. 196p. New York: Pergamon; 1986. DOI: 10.1007/978-0-7506-2633-0

[18] Guyer RA. The theory of quantum crystals. In: Seitz F, Tumbull D, Ehrenreich H, editors. Solid State Physics. Vol. 23. New York: Academic Press; 1969. pp. 413-499. DOI: 10.1016/S0081–1947(08)60618–9

[19] Ebner C, Sung CC. Correlation effects in quantum crystals. Physical Review A. 1971;**4**:269-281. DOI: 10.1103/PhysRevA.4.269

[20] Gov N, Polturak E. Local modes, phonons, and mass transport in solid ^{4}He. Physical Review B. 1999;**60**: 1019-1027. DOI: 10.1103/PhysRevB.60.1019

[21] Greywall DS. Elastic constants of hcp ^{4}He. Physical Review B. 1977;**16**: 5127-5128. DOI: 10. 1103/PhysRevB.16.5127

[22] Day JP, Ruoff AL. The variation of the elastic constants of lithium with temperature and pressure. Physica Status Solidi. 1974;**25**:205-213. DOI: 10.1002/pssa.2210250118

[23] Tromans D. Elastic anisotropy of hcp metal crystals and polycrystals. International Journal of Research and Reviews in Applied Sciences. 2011;**6**: 462-483. Available from: https://arpapress.com/Volumes/Vol 6Issue4/IJRRAS_6_4_14.pdf

[24] Flugge S. Practical Quantum Mechanics. 2nd ed. Berlin: Springer; 1999. p. 635. DOI: 10.1007/978-3-642-61995-3

[25] Guyer RA, Richardson RC, Zane LI. Excitations in quantum crystals (A survey of NMR experiments in solid helium). Reviews of Modern Physics. 1971;**43**:532-600. DOI: 10.1103/RevModPhys.43.532

[26] Andreev AF. Diffusion in quantum crystals. Soviet Physics Uspekhi. 1976; **19**:137-148. DOI: 10.1070/PU1976v019n02ABEH005133